CEMCAP

Co-funded by the European Union

Grant Agreement Number:
641185

Action acronym:
CEMCAP

Action full title:
CO_2 capture from cement production

Type of action:

H2020-LCE-2014-2015/H2020-LCE-2014-1

Starting date of the action: 2015-05-01
Duration: 42 months

D12.4
CaL reactor modelling and process simulations

Due delivery date: 2017-10-31
Actual delivery date: 2017-10-31

Organization name of lead participant for this deliverable:
Politecnico di Milano (PoliMi)

Project co-funded by the European Commission within Horizon2020		
Dissemination Level		
PU	Public	x
CO	Confidential , only for members of the consortium (including the Commission Services)	

Deliverable number:	D12.4
Deliverable title:	CaL reactor modelling and process simulations
Work package:	WP12: Calcium looping capture
Lead participant:	USTUTT

Author(s)		
Name	**Organisation**	**E-mail**
Maurizio Spinelli	Politecnico di Milano	maurizio.spinelli@polimi.it
Edoardo de Lena	Politecnico di Milano	edoardo.delena@polimi.it
Matteo Romano*	Politecnico di Milano	matteo.romano@polimi.it

*Lead author

Keywords

CO_2 capture, Calcium looping, entrained flow reactor, cement

Abstract

The aim of this deliverable is to present the models and some representative results from the simulations of the CaL reactors system for CO_2 capture in cement plant. The following two CaL reactor systems are assessed:

1. Circulating fluidized bed CaL for Tail End CaL configuration
2. Entrained flow reactors for highly integrated CaL configuration

Mass and energy balances of the two CaL reactor technologies are calculated with Matlab codes and will be used for the process integration work of WP4.

The results obtained indicate that with CFB reactors, CO_2 capture efficiency >90% is easily achievable. The large limestone make-up flow available in cement kilns allows operating with a highly active sorbent in the carbonator, which facilitates the achievement of the 90% capture target. With entrained flow reactors, simulations indicate that CO_2 capture efficiency in the carbonator of around 80% (i.e. about 90% capture efficiency for the whole cement kiln) can be achieved with sufficiently high solid to gas ratio. Sorbent capacity, which may highly depend on the raw meal nature and on the calcination conditions, highly influence the solid/gas ratio needed to achieve the target CO_2 capture efficiency.

This project has received funding from the European Union's Horizon2020 Research and Innovation Programme under Grant Agreement No 641185

TABLE OF CONTENTS

Page

This project has received funding from the European Union's Horizon2020 Research and Innovation Programme under Grant Agreement No 641185

NOMENCLATURE

A	Reactor cross section [m^2]
C_{CO_2}	CO_2 concentration in gas phase [$kmol/m^3$]
$C_{CO_2,eq}$	CO_2 concentration in gas phase at chemical equilibrium with CaO-$CaCO_3$ [$kmol/m^3$]
c_p	Specific heat capacity [J/kg/K]
D	Reactor diameter [m]
D_p	Particle diameter [m]
F_{fg}	Gas-wall friction force per unit of reactor length [N/m]
F_{fs}	Solid-wall friction force per unit of reactor length [N/m]
f_g	Fanning friction factor [-]
F_{gs}	Gas-solid drag force per unit of reactor length [N/m]
Fe	Fedorov number [-]
g	Gravitational acceleration: 9.81 m/s^2
h	Sensible enthalpy [J/kg]
h_{gs}	Heat transfer coefficient between gas and solids [$W/m^2/K$]
I_G	Gravitational acceleration sign index: +1 for upward flow, -1 for downward flow
M	Molar mass [kg/kmol]
$\dot{M}$	Mole flow rate [kmol/s]
$\dot{m}$	Mass flow rate [kg/s]
N_s	Number of solid particles per unit of reactor volume [m^{-3}]
Nu_{gs}	Nusselt number related to the gas-solid heat transfer coefficient [-]
p	Pressure [Pa]
Pr	Prandtl number [-]
$\dot{q}_{CO2,carb}$	Thermal power associated to the enthalpy flow of the reacting CO_2 per unit of reactor length [W/m]
$\dot{q}_{gs}$	Thermal power transferred from the gas to the solids per unit of reactor length [W/m]
$\dot{q}_{gw}$	Thermal power transferred from the gas to the reactor wall per unit of reactor length [W/m]
$\dot{q}_{r,carb}$	Thermal power associated to the carbonation reaction per unit of reactor length [W/m]
$\dot{q}_{sw}$	Thermal power transferred from the solids to the reactor wall per unit of reactor length [W/m]
Re	Reynolds number of the gas in the reactor [-]
Re_p	Particle Reynolds number [-]
S	Specific surface area available for carbonation reaction in the particle [m^2/m^3]
T	Temperature [K]
u	Velocity [m/s]
$\dot{w}_{gs}$	Work per unit length made by the gas on the solids [W/m]
x	Axial coordinate [m]
X	Sorbent conversion degree [-]
X_{max}	Sorbent conversion degree after the fast kinetically controlled period [-]

This project has received funding from the European Union's Horizon2020 Research and Innovation Programme under Grant Agreement No 641185

Greek letters

ε_p	Particle porosity [$m^3_{void}/m^3_{particle}$]
ε_s	Volumetric solid density [$m^3_{solids}/m^3_{reactor}$]
ε_g	Void fraction [$m^3_{gas}/m^3_{reactor}$]
ξ	Volume ratio between the potentially active solids (CaO and $CaCO_3$) and the total solid population [$m^3_{CaO\&CaCO3}/m^3_{solids}$]
ρ	Density [kg/m^3]
ψ	Particle structural parameter for random pore kinetic model

Acronyms

ASU	Air separation unit
CaL	Calcium looping
CPU	CO_2 purification unit
IL	Integration level

This project has received funding from the European Union's Horizon2020 Research and Innovation Programme under Grant Agreement No 641185

1 TAIL END CAL CONFIGURATION

In the Tail End CaL configuration, two interconnected circulating fluidized bed (CFB) reactors are considered for the carbonator and the calciner. The CaL system is integrated in the cement kiln as shown in Figure 1.1, where the main component of the conventional cement kiln and the CaL CO_2 capture system are highlighted. In the proposed layout, the carbonator is used as an end-of-pipe CO_2 sorption unit from the gases coming from the preheating tower of cement kiln.

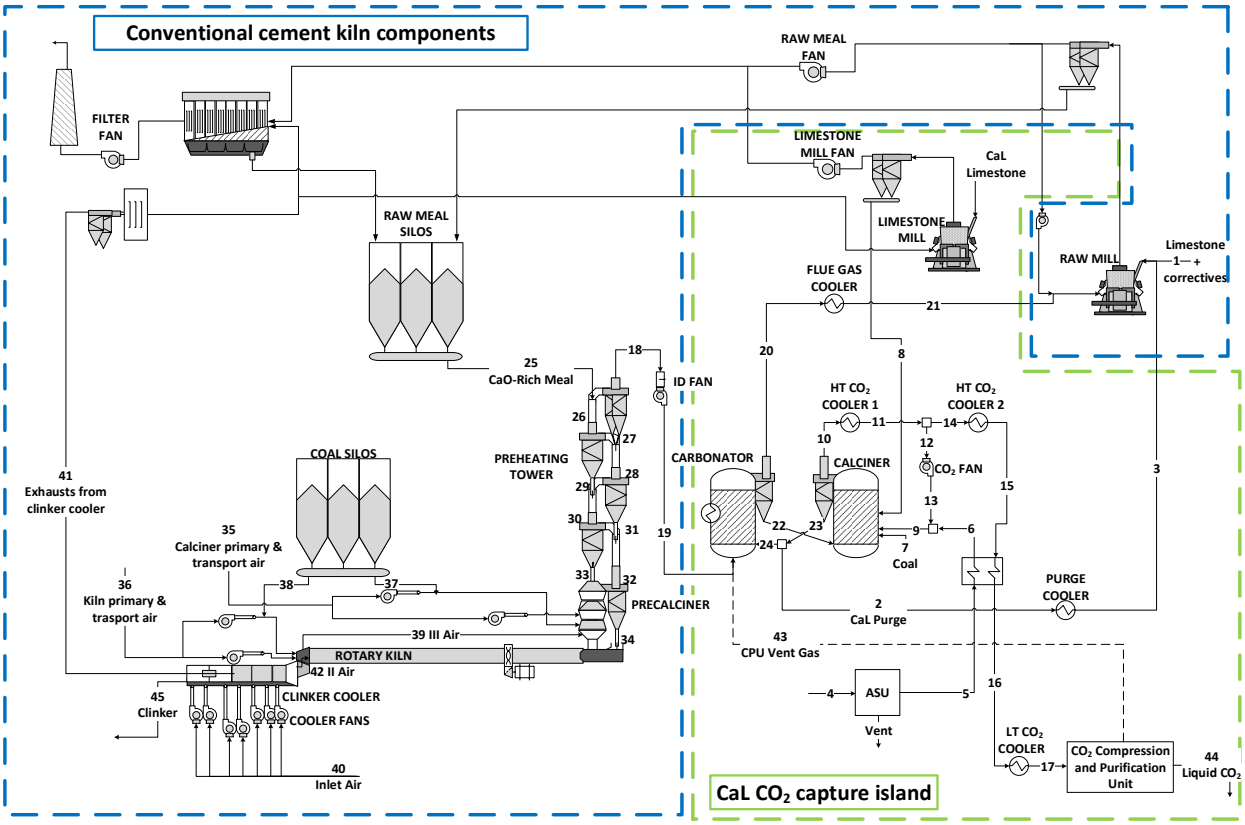

Figure 1.1: Process flowsheet of the tail-end CaL process integration for CO_2 capture in a cement kiln

The integration between the cement kiln and the CaL system is done through the flue gases exiting the preheater tower of the cement kiln (stream #19), which are fed to the carbonator of the CaL system, and the CaO-rich solid purge (#2) from the calciner of the CaL system, which replaces part of the raw meal limestone as source of calcium for clinker production.

The purge stream from the CaL system is cooled down from 920°C to 80°C and it is fed to the raw meal mill of cement kiln where it is mixed with additional limestone and correctives (#1), ground and dried, using the hot decarbonized gas from carbonator, before being fed to the preheating tower.

In this configuration, high purity limestone (#8) is used as CO_2-sorbent and it is fed to the calciner of the CaL process. The amount of CO_2-sorbent fed to the calciner of the CaL can be represented through the ratio F_0/F_{CO2}, which indicates the molar flow of $CaCO_3$ fed to the calciner per mole of CO_2 entering the carbonator of the CaL. In the calciner reactor, oxycombustion of coal (#7) is carried out for supplying the energy needed for $CaCO_3$ calcination. The calciner operating temperature is 920°C, which provides a sufficient driving force to calcination reaction to assume that $CaCO_3$ is completely calcined (i.e. 100% calcination degree) in the oxyfuel calciner [MAR, 2013]. Higher calcination temperature than in the pre-

This project has received funding from the European Union's Horizon2020 Research and Innovation Programme under Grant Agreement No 641185

calciner (860°C) of the cement kiln is needed to allow calcination under the higher CO_2 partial pressure conditions in this reactor. Coal used as fuel in the cement plant contains CaO in the ash, which contribute to provide the calcium needed for clinker production. The amount of CaO from coal ashes is non-negligible under some operating conditions (the ash content in the coal is 16.5%wt., and the CaO content in the ash is 18.2%wt. as discussed in CEMCAP Deliverable D4.1). CaO originating from coal ash has been considered as inactive in the CaL process. As shown in Figure 1.1, the amount of $CaCO_3$ and ash introduced in the CaL calciner is ultimately extracted as CaO-rich CaL purge and sent to clinker production process. The *integration level* (IL) is defined as the fraction of Ca entering the clinker burning line with the CaL purge stream with respect to the total Calcium fed to the plant.

After the specific make-up ratio F_0/F_{CO2}, another important parameter for solving the CaL balances is the ratio F_{Ca}/F_{CO2}, which indicates the ratio between the CaO molar flow rate flowing from the CaL calciner to the carbonator and the molar flow of CO_2 entering this reactor with the exhaust gas from the cement kiln.

The third important process parameter for the CaL system is the solid inventory (W_s). For given values of F_0/F_{CO2} and F_{Ca}/F_{CO2}, higher W_s lead to higher CO_2 capture rates but also to higher gas pressure drops and fan consumption. An inventory W_s of 1000 kg per m^2 of carbonator cross-section is considered in this analysis.

1.1 Carbonator model description

The carbonator model developed by Romano [ROM, 2012] is used for calculating the CO_2 capture efficiency (E_{carb}). This model considers the carbonator as an isothermal circulating fluidized bed reactor based on the Kunii-Levenspiel model [KUN, 1997] and includes the carbonation kinetic expression proposed by Grasa et al. in [GRA, 2008], corrected to take the effect of coal ash and sulphur into account. This model allows calculating CaO conversion in carbonator (X_{carb}), as a function of main operating conditions in the reactor, the CaO particle proprieties and the amount of ash and sulphur in the coal burned in the calciner. The CO_2 capture efficiency in the carbonator E_{carb} can be calculated according to eq.1.

$$E_{carb} = \frac{F_{Ca} \cdot X_{carb}}{F_{CO2}} \tag{1}$$

As a matter of comparison, the ideal carbonator efficiency is also calculated assuming that CaO particles achieve their maximum conversion (X_{max}) in the carbonator. In this ideal situation, E_{carb} is limited either by the equilibrium of the carbonation reaction (i.e. by the equilibrium CO_2 partial pressure in the gas phase at the assumed carbonator temperature) or by the flow of CaO entering the carbonator. This maximum theoretical carbonator capture efficiency can be calculated according to eq.2, where X_{max} is estimated using eq.3 considering the semi-empirical CaO capacity decay law proposed in [GRA, 2006], with a decay constant k of 0.52 and residual capacity (X_r) of 0.075, and the statistical cycle number distribution (r_N) calculated by eq.4 [ABA, 2002].

$$E_{carb} = \min\left(\frac{F_{Ca} \cdot X_{max}}{F_{CO2}}; E_{eq}\right) \tag{2}$$

$$X_{max} = \sum_{N=1}^{\infty} r_N \cdot \left(\frac{1}{\frac{1}{(1-X_r)} + k \cdot N} + X_r\right) \tag{3}$$

This project has received funding from the European Union's Horizon2020 Research and Innovation Programme under Grant Agreement No 641185

$$r_n = \frac{F_0 \cdot F_{Ca}^{N-1}}{(F_0 + F_{Ca})^N} \quad (4)$$

1.2 Process simulation results

Figure 1.2 shows the CO_2 capture efficiency attained in the carbonator for ILs of 15, 20 and 25%. Capture efficiency curves, calculated by the model developed by Romano [ROM, 2012], are compared with the ideal capture rate calculated by Eq(2-4), which correspond to the cases with the maximum conversion of CaO particles.

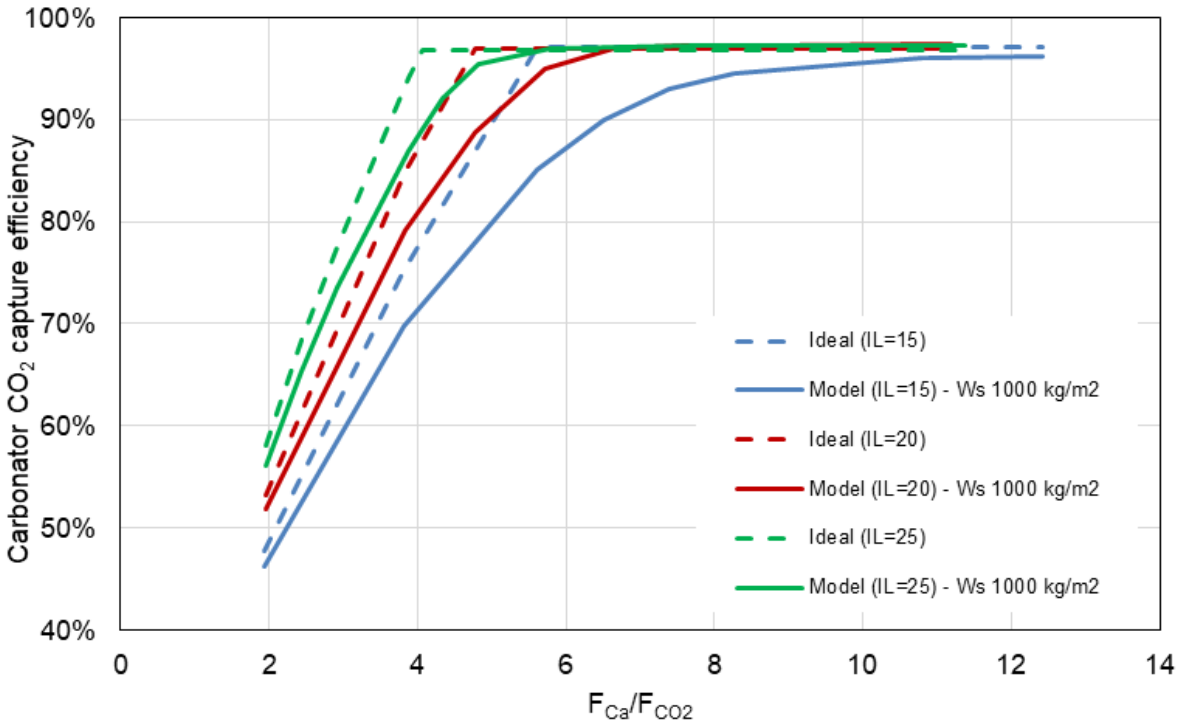

Figure 1.2: Carbonator CO_2 capture efficiency as a function of the F_{Ca}/F_{CO2} ratio and the integration level IL.

As mentioned before, high ILs lead to high sorbent make-up (F_0/F_{CO2}) and therefore to highly active CaO sorbent in CaL system. Furthermore, when IL value increases, the amount of solids purged from the system increases, reducing the amount of ash and sulphur in the solid population and the average number of calcination-carbonation cycles experienced by CaO particle. Both effects favor the average reactivity of the solid population, which leads to higher E_{carb}.

The curves shown in Figure 1.2 can be divided into two regions. In the first region, at low value of the sorbent circulation rate F_{Ca}/F_{CO2}, the CO_2 capture efficiency is limited by the active sorbent availability. In the second region, at high F_{Ca}/F_{CO2}, the capture efficiency is limited by the thermodynamic equilibrium of the carbonator reaction. The maximum theoretical capture efficiency of about 96%, corresponding to the theoretical upper bound for E_{carb}, is achieved in the ideal cases and a sharp transition between the two different regions is noticed. When the carbonator model is used a smooth transition is noticed, indicating that carbonator performance is limited by carbonation reaction kinetics and mass transport when active sorbent circulation is close to the stoichiometric one.

This project has received funding from the European Union's Horizon2020 Research and Innovation Programme under Grant Agreement No 641185

The CaL reactor system has been simulated by combining the carbonator reactor model developed in Matlab and the CaL reactors system developed with the in-house software GS [GS, 2016]. The main assumptions adopted for these simulations are reported in Table 1.1.

Table 1.1: Main assumptions for the calculation of the CaL system in the Tail End configuration.

Ca-Looping process	
Carbonator outlet temperature [°C]	650
Carbonator solid inventory [kg/m^2]	1000
Gas superficial velocity at carbonator inlet [m/s]	5
Calciner outlet temperature [°C]	920
Recycle gas temperature [°C]	400
Oxygen concentration in oxidant flow to calciner [%vol.]	50
Oxygen preheating temperature [°C]	150
Oxygen concentration in calciner off-gas [%vol.]	5

The carbonator reactor is operated at the typical temperature of 650°C [MAR, 2016] and the operating temperature of calciner is assumed equal to 920°C to guarantee a complete calcination of $CaCO_3$ with a high CO_2 partial pressure conditions.
A cryogenic Air Separation Unit (ASU) produces 95% pure oxygen to be used as oxidant in the CaL calciner. A CO_2-rich recycle at 400°C has been considered as temperature moderator and fluidizing gas, whose flow rate is controlled to have an O_2 concentration in the oxidant stream at calciner inlet of 50% on a molar basis.
As for the fluidized beds hydrodynamics, the minimum specific solid flow rate ($G_{s,min}$) needed to ensure solids circulation between the two reactors has been calculated. For both the carbonator and the calciner, the reactors cross section is computed by assuming a superficial gas velocity of 5 m/s. $G_{s,min}$ is therefore computed as the ratio between the mass flow rate of the solids flowing between the reactors and the cross-section of the reactor where such solids come from. Figure 1.3 shows $G_{s,min}$ as a function of IL and F_{Ca}/F_{CO2}. For F_{Ca}/F_{CO2} ratios in the CaL system between 4 and 6, minimum solid circulations are in the range of 8-17 kg/(m^{2}s) and of 4-7 kg/(m^{2}s) for the carbonator and calciner respectively. These values of $G_{s,min}$ are in the range of the typical solid circulation of commercial CFB combustors, indicating that the solid circulation can be entirely sustained by the transport capacity of the gas in the reactors. As can be seen from Figure 1.2, at F_{Ca}/F_{CO2} of 4-6, carbon capture efficiencies between 70% and >95% are feasible in the carbonator of the CaL system depending on the IL.

This project has received funding from the European Union's Horizon2020 Research and Innovation Programme under Grant Agreement No 641185

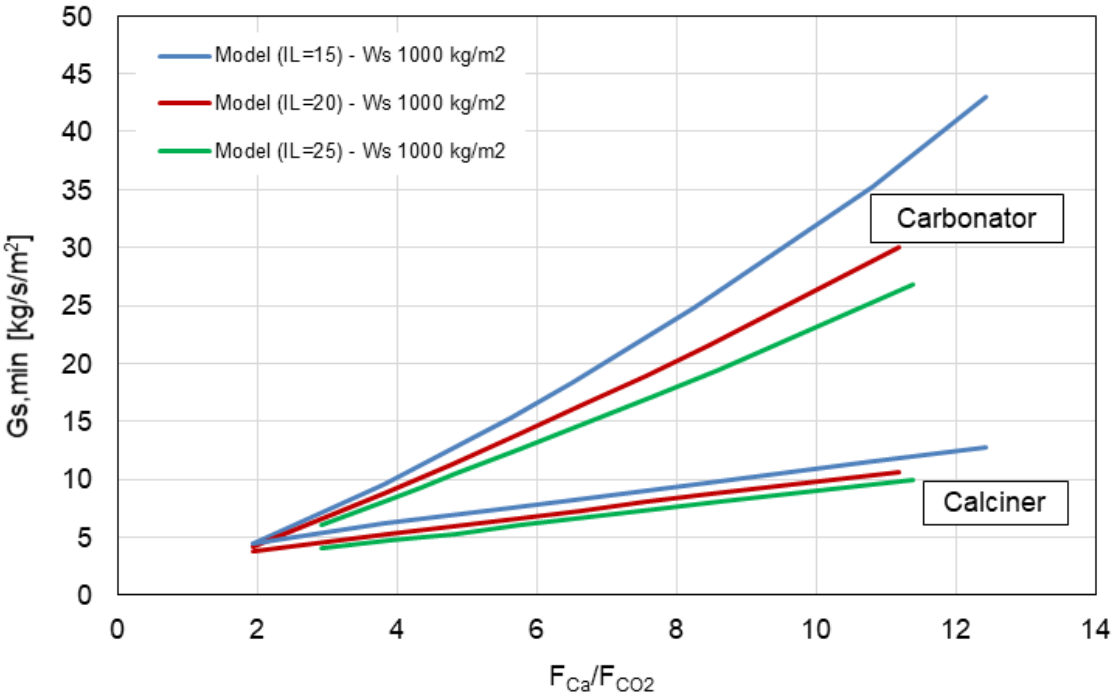

Figure 1.3: Minimum solid circulation in the reactors of the CaL system as a function of the Integration Level (IL) and the CaO circulation rate (F_{Ca}/F_{CO2})

Finally, Figure 1.4 shows the fuel consumption in rotary kiln, pre-calciner and CaL calciner for the reference cement kiln without CO_2 capture (first bar) and for the CaL cement kiln with IL between 15 and 80%, calculated with the process integration calculations presented in [DEL, 2017]. In the case without CO_2 capture, the fuel consumed in the rotary kiln is about 38% of the total heat input and it corresponds to 1.22 MJ_{LHV}/kg_{clk}, whereas the coal entering the pre-calciner provides a heat input of 2.00 MJ_{LHV}/kg_{clk}. The total fuel thermal input increases by 95-210% when the tail-end CaL process is integrated in the cement kiln. Fuel consumption in the calciner of the CaL process accounts for about 70-80% of the total fuel consumption of the plant, which corresponds to 150 to 220% of the fuel consumption in the base case. Fuel consumption in the pre-calciner reduces by 17% for IL 15% to 93% for IL 80%, compared to the base case.
The reason for the large increase of fuel consumption is intrinsic in the tail-end configuration, because the CO_2 released in the pre-calciner from the raw meal calcination results in the formation of $CaCO_3$ in the carbonator of the CaL process, which is calcined again in the oxyfuel calciner. This double calcination step, needed for capturing the molecules of CO_2 originally in the limestone fed to the pre-calciner of the cement kiln, involves significant overall fuel consumption. This double calcination effect reduces if IL increases because limestone fed to the CaL calciner is subject to a single oxyfuel calcination process. This is the reason why the lowest overall fuel consumption has been obtained for the case with IL=80%.

This project has received funding from the European Union's Horizon2020 Research and Innovation Programme under Grant Agreement No 641185

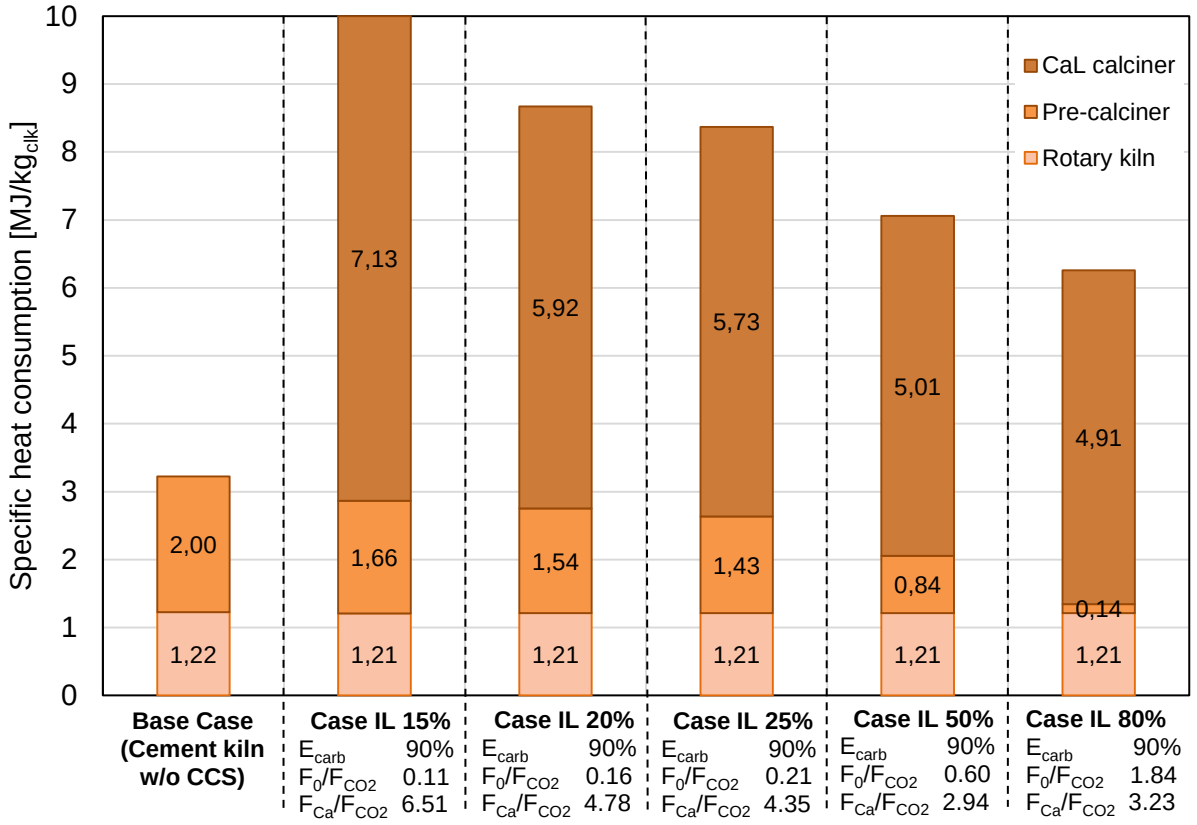

Figure 1.4: Specific fuel consumption in rotary kiln, pre-calciner and CaL calciner for the reference cement kiln without CO_2 capture (first bar) and for the CaL cement kiln with different ILs.

It has to be remarked that the high fuel consumption of the tail-end CaL configuration result in high heat available for the bottoming steam cycle which can produce enough electricity to compensate the electric consumption for oxygen production and CO_2 compression. Consequently, indirect emissions and indirect fuel consumption associated to the electric balance of the plant will reduce and may become negative (i.e. fuel and emissions credits) in case electricity is exported to the grid. Therefore, high fuel consumption does not necessarily involve high overall energy penalties, as discussed in [DEL, 2017] and further addressed in Cemcap WP4.

This project has received funding from the European Union's Horizon2020 Research and Innovation Programme under Grant Agreement No 641185

2 INTEGRATED CAL CONFIGURATION

This section presents the assessment of the Integrated CaL configuration based on entrained flow carbonator in the cement kiln. Differently from the tail-end configuration, in this case the CaO-rich sorbent is constituted by the calcined raw meal used for clinker production, hence it contains also silica, alumina and ferritic species which are normally present in the raw meal fed to the preheating tower. In addition, the average sorbent particle size is lower (≈10-30 µm vs. ≈ 200-300 µm in the CFB carbonator of the tail end case), which drives the adoption of entrained flow CaL reactors. The configuration of the proposed solution is represented in Figure 2.1.

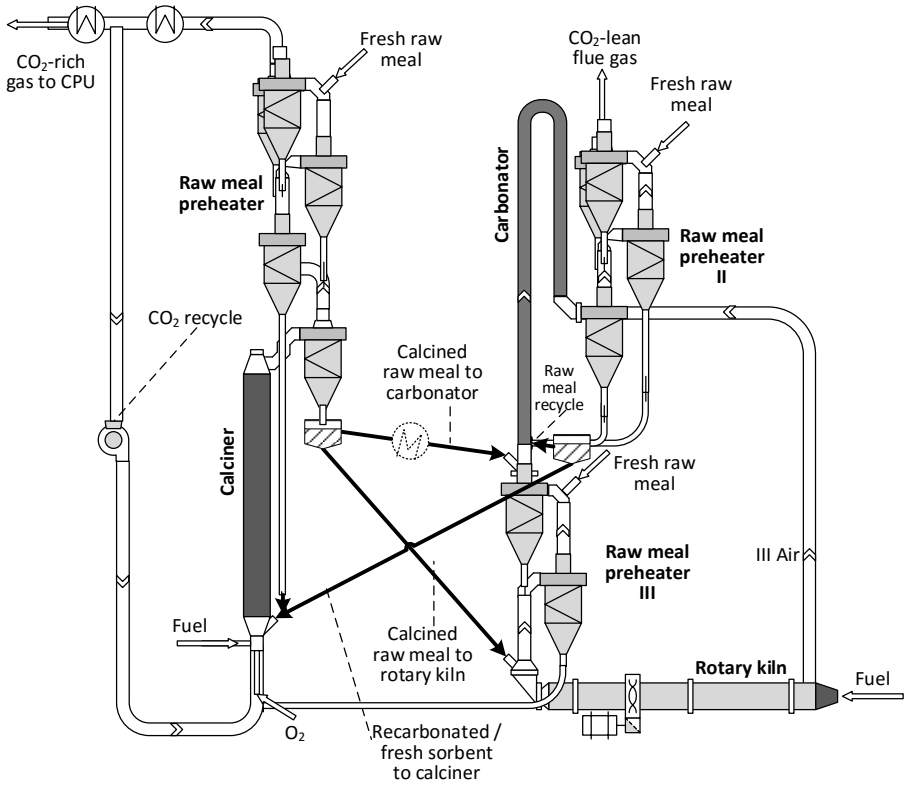

Figure 2.1: Highly integrated CaL configuration with a gooseneck-type entrained flow carbonator

The integrated CaL process is based on the idea of switching the pre-calciner to oxyfuel operation, so that the carbon coming from fuel combustion and calcium carbonate decomposition is recovered as a high concentrated stream of CO_2, suitable for compression and storage processes. A variable portion of the calcined material produced in the oxyfuel calciner is sent to the entrained flow carbonator, which can be designed as a long reactive gooseneck reactor integrated with the preheating tower. The remaining amount of calcined raw meal is introduced in the rotary kiln. From the CaL system perspective, this second stream represents the sorbent purge, while the entire raw meal fed to the preheating tower represents the sorbent make-up.

Before entering the carbonator, the CO_2-rich exhausts leaving the rotary kiln are fed to a two-stage suspension preheater to reduce the gas temperature. The CO_2-lean gases at the carbonator outlet are mixed with the hot air from the clinker cooler (i.e. the tertiary air of conventional cement kilns) and used for further raw meal preheating and steam generation.

This project has received funding from the European Union's Horizon2020 Research and Innovation Programme under Grant Agreement No 641185

2.1 Carbonator model description

A one-dimensional, steady-state model has been developed for the calculation of the entrained flow carbonator. The routine solves mass, energy and momentum balances along the axial direction for the gas and solid phases, providing cross-sectional averaged values of their chemical composition, temperature and velocity.
The main assumptions used to build the model are listed below:

- The gas phase is modelled with the ideal gas equation of state.
- Since the reactor operates with a dilute suspension, particle-particle interactions are neglected in the calculation of the momentum balance.
- The mass and momentum diffusion and the conductive heat flux along the axial direction are neglected.
- Uniform temperature is considered for the solid throughout the particle.

A forward finite difference method has been implemented in Matlab to solve the equations presented in the following section along the reactor length. The possibility of recycling a portion of the solids collected by the cyclone at the carbonator outlet back to the inlet of the reactor is implemented. In this case, an iterative calculation is implemented, where solid composition and flow rate at the inlet section are updated until convergence is achieved.

2.1.1 Mass and energy balances

Mass balance of solids and gas phases is described by equations 5 and 6, where the change of flow rate along the reactor length is related to the mass flow rate of CO_2 absorbed by the sorbent. In details, Equations 5 states that the variation of solids mass flow rate $d\dot{m}_s$ is equal to the number of moles of active sorbent in an infinitesimal control volume $A \cdot dx \cdot \frac{\varepsilon_s \cdot \xi \cdot \rho_{s,a}}{M_{s,a}}$, multiplied by the sorbent molar conversion rate $\frac{dX}{dt}$ and the CO_2 molar mass.

$$\frac{d\dot{m}_s}{dx} = A \cdot \frac{\varepsilon_s \cdot \xi \cdot \rho_{s,a}}{M_{s,a}} \cdot \frac{dX}{dt} \cdot M_{CO2} = \frac{\xi \cdot \dot{m}_s \cdot \rho_{s,a}}{u_s \cdot \rho_s \cdot M_{s,a}} \cdot \frac{dX}{dt} \cdot M_{CO2} = \frac{\dot{M}_{s,a}}{u_s} \cdot \frac{dX}{dt} \cdot M_{CO2} \quad (5)$$

$$\frac{d\dot{m}_g}{dx} = -\frac{d\dot{m}_s}{dx} \quad (6)$$

For the sorbent conversion rate, the random pore model equation 7 proposed by Grasa et al. [GRA, 2009] is used, which describes the sorbent reaction rate in the fast kinetically controlled period. The use of this equation, neglecting the diffusion controlled particle conversion, is justified given the small residence time of the particles in the entrained flow reactor.

$$\frac{dX}{dt} = \frac{k_s \cdot S}{1-\varepsilon_p} \cdot (1-X) \cdot \sqrt{1-\psi \cdot ln(1-X)} \cdot \left(C_{CO_2} - C_{CO_2,eq}\right) \quad (7)$$

Momentum balance is written for the gas and the solid phases as shown in equations 8 and 9, following the approach of Rajan et al. [RAJ, 2006]. In these equations I_G is an index representing the sign of the gravitational acceleration with respect to the flow direction and is equal to +1 in case of upward flow and -1 in case of downward flow, F_{fg} and F_{fs} are the gas-wall and the solid-wall friction forces and F_{gs} is the gas-solid drag force per unit of reactor length.

This project has received funding from the European Union's Horizon2020 Research and Innovation Programme under Grant Agreement No 641185

$$\frac{d(\dot{m}_g \cdot u_g)}{dx} + A \cdot \frac{dp}{dx} = -I_G \cdot A_g \cdot \rho_g \cdot g - F_{fg} - F_{gs} \quad (8)$$

$$\frac{d(\dot{m}_s \cdot u_s)}{dx} = -I_G \cdot A_s \cdot \rho_s \cdot g - F_{fs} + F_{gs} \quad (9)$$

Energy balance is written for the gas and the solid phases as shown in equations 10 and 11. Changes of total energy of the gas phase per unit of reactor length are related to the work per unit length made by the gas on the solids ($\dot{w}_{gs}$), to the thermal power transferred from the gas to the solids ($\dot{q}_{gs}$), from the gas to the reactor wall ($\dot{q}_{gw}$) and from the solids to the reactor wall ($\dot{q}_{sw}$) per unit of reactor length, to the thermal power generated by the carbonation reaction ($\dot{q}_{r,carb}$) and to the enthalpy flow associated to the reacting CO_2 ($\dot{q}_{CO2,carb}$).

$$\frac{d\left(\dot{m}_g \cdot h_g + 0.5 \cdot \dot{m}_g \cdot u_g^2 + I_G \cdot \dot{m}_g \cdot g \cdot x\right)}{dx} = -\dot{w}_{gs} - \dot{q}_{gw} - \dot{q}_{gs} - \dot{q}_{CO2,carb} \quad (10)$$

$$\frac{d(\dot{m}_s \cdot h_s + 0.5 \cdot \dot{m}_s \cdot u_s^2 + I_G \cdot \dot{m}_s \cdot g \cdot x)}{dx} = \dot{w}_{gs} - \dot{q}_{sw} + \dot{q}_{gs} + \dot{q}_{r,carb} + \dot{q}_{CO2,carb} \quad (11)$$

Gas to solids heat transfer is calculated with equation 12, where N_s is the number of solid particles per unit of reactor volume, calculated with eq. 13. Only convective heat transfer is considered in the model to calculate the gas-solid heat transfer coefficient h_{gs}, which is estimated through the gas-solid Nusselt number Nu_{gs} with empirical equation 14 [RAJ, 2008].

$$\dot{q}_{gs} = A \cdot N_s \cdot \pi \cdot D_p^2 \cdot h_{gs} \cdot \left(T_g - T_s\right) \quad (12)$$

$$N_s = \frac{6 \cdot A_s}{A \cdot \pi \cdot D_p^3} \quad (13)$$

$$Nu_{gs} = 8.2951 \cdot 10^{-7} \cdot Re_p^{5.3365} \cdot \left(\frac{\dot{m}_s}{\dot{m}_g}\right)^{-1.3863} \cdot Fe^{-5.053} \quad (14)$$

For calculating the heat transfer with the reactor wall, particles to wall heat transfer $\dot{q}_{sw}$ is assumed zero, while gas to wall heat transfer $\dot{q}_{gw}$ is calculated with equation 15, where the enhancement provided by the presence of the solid particles is considered. Gas to wall heat transfer coefficient h_{gw} is computed from Nu_{gw} in equation 16, where the first term between brackets from the Dittus-Boelter correlation is increased by the second term, which includes the ratio of the heat capacities of solids and gas streams [PFE, 1966].

$$\dot{q}_{gw} = A \cdot h_{gw} \cdot \left(T_g - T_w\right) \quad (15)$$

$$Nu_{gw} = (0.023 \cdot Re^{0.8} \cdot Pr^{0.3}) \cdot \left(1 + 4 \cdot Re^{-0.32} \cdot \frac{\dot{m}_s}{\dot{m}_g} \cdot \frac{c_{p,s}}{c_{p,g}}\right) \quad (16)$$

This project has received funding from the European Union's Horizon2020 Research and Innovation Programme under Grant Agreement No 641185

2.2 Process simulations results

A sensitivity analysis has been performed on the EF CaL system with the assumptions reported in Table 2.1. A maximum CaO conversion (X_{max}) of 0.2 in the kinetic controlled conversion period has been assumed. As highlighted in calcination-carbonation tests in labs in Cemcap WP12, this value is highly dependent on the raw meal nature and on the calcinations conditions and it is difficult to predict with the current knowledge and experimental data. Therefore, a sensitivity analysis has been performed on this parameter. For the calciner, an outlet temperature of 920°C has been assumed to calculate the heat input needed in that reactor to heat up and calcine the recarbonated raw meal from the carbonator.

Table 2.1: Assumptions for the simulation of the entrained flow CaL carbonator.

Gas flow rate, kg/s Nm^3/s	17.06 12.44
CO_2 concentration in the gas, %vol.	19.8
Sorbent composition, %wt.	65.5CaO, 0.2$CaCO_3$, 21.6SiO2, 5.0Al_2O_3, 2.7Fe_2O_3, 2.4MgO, 2.6$CaSO_4$
Maximum CaO conversion (X_{max})	0.20
Particle size, µm	30
Gas inlet velocity, m/s gooseneck reactor downflow reactor	 15 4
Initial solid velocity, m/s	1
Reactor inlet temperature, °C	600
Reactor wall temperature, °C	300
Calciner outlet temperature, °C	920

In Figure 2.2, the CO_2 capture efficiency vs. reactor length, for adiabatic and cooled reactor and different solid/gas ratio is shown for a gooseneck reactor. As shown in the chart, a solid to gas ratio of around 10 kg/Nm^3 is needed to achieve a CO_2 capture efficiency of 80% (i.e. about 90% capture efficiency for the whole cement kiln) with a reactor length of 120-140 m.
In Figure 2.2 it is also shown that cooled reactors allow achieving higher capture efficiencies, especially when 4 parallel cooled reactors are used to increase the reactor surface/volume ratio. However, the effect of reactor cooling is moderate, allowing to increase the capture efficiency by about 6-8% points in case of 4 parallel reactors and by about 5-6% points in case of single cooled reactor, compared to the adiabatic reactor case. It is believed that such improvement of the capture efficiency does not justify the increased cost associate to a waterwall cooled reactor and therefore adiabatic reactors appear preferable from the techno-economic point of view.

This project has received funding from the European Union's Horizon2020 Research and Innovation Programme under Grant Agreement No 641185

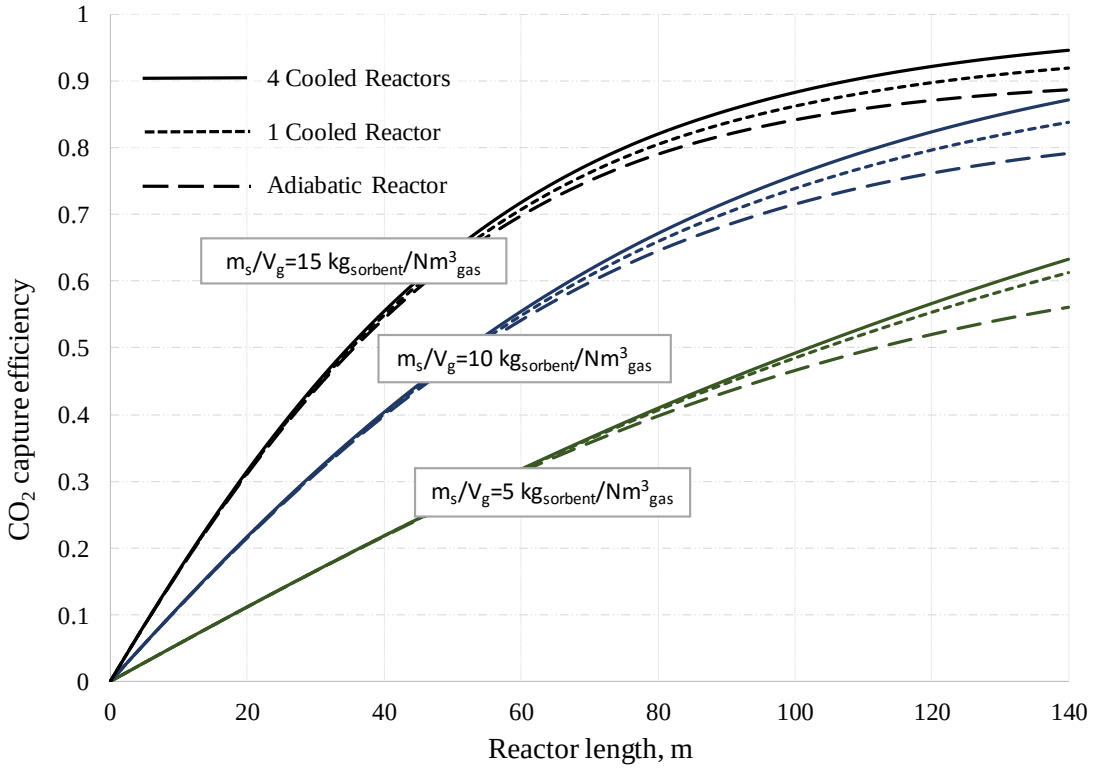

Figure 2.2: CO_2 capture efficiency vs. reactor length, for adiabatic and cooled reactor and different solid/gas ratio (Xmax=20%, inlet temperature = 600°C, no solids recycle).

In Figure 2.2, only pre-calcined solids from the oxyfuel CaL calciner are assumed to be fed to the carbonator. This means that increasing the solid loading in the carbonator also significantly increases the heat to be provided in the calciner. To keep a proper solid loading in the carbonator without increasing the solid flow from the calciner to the carbonator, a solid recycle from carbonator outlet to carbonator inlet can be adopted. The results of the simulations with such operating condition is shown in Figure 2.3, where a solid circulation from calciner to carbonator of 5 kg/Nm^3 is maintained, while solid loading at carbonator inlet is increased up to about 10 and 15 kg/Nm^3 by recycling 1/2 and 2/3 of the solids at carbonator outlet. Because the solids at carbonator inlet are partly carbonated, CO_2 capture efficiency in this case is lower than in the cases without recycle and the same solid loading. CO_2 capture efficiency between 75 and 82% can be obtained with recycle rate between 50 and 67% with adiabatic reactor.
In Figure 2.4, the effect of sorbent capacity X_{max} is shown for adiabatic carbonator with 50% and 66.7% recycle. The impact of sorbent capacity is significant. If sorbent capacity reduced to 10%, CO_2 capture efficiency of only 50% would be achieved in a 140 m reactor and 66.7% of solid recycle. On the other hand, if sorbent capacity increased to 30%, 80% capture efficiency would be more easily achieved with a reactor length between 65 and 100 m, depending on the solid loading.

This project has received funding from the European Union's Horizon2020 Research and Innovation Programme under Grant Agreement No 641185

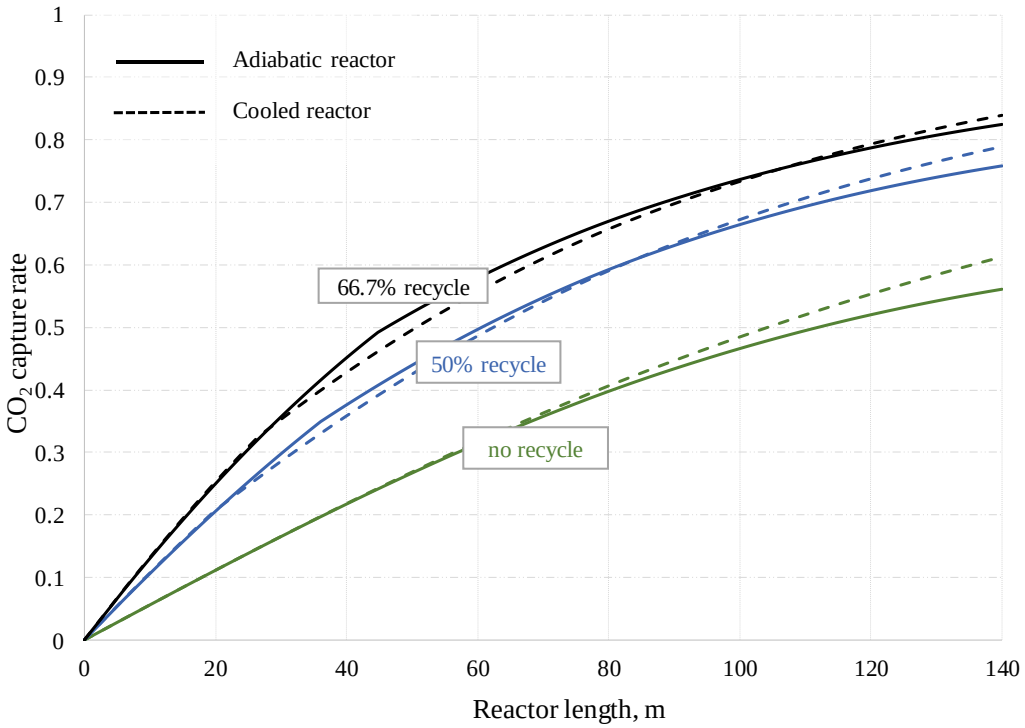

Figure 2.3: CO_2 capture efficiency vs. reactor length, for adiabatic and cooled reactor, solid feeding from the calciner of 5 kg/Nm^3 and different recycle ratios (X_{max}=20%, inlet temperature = 600°C).

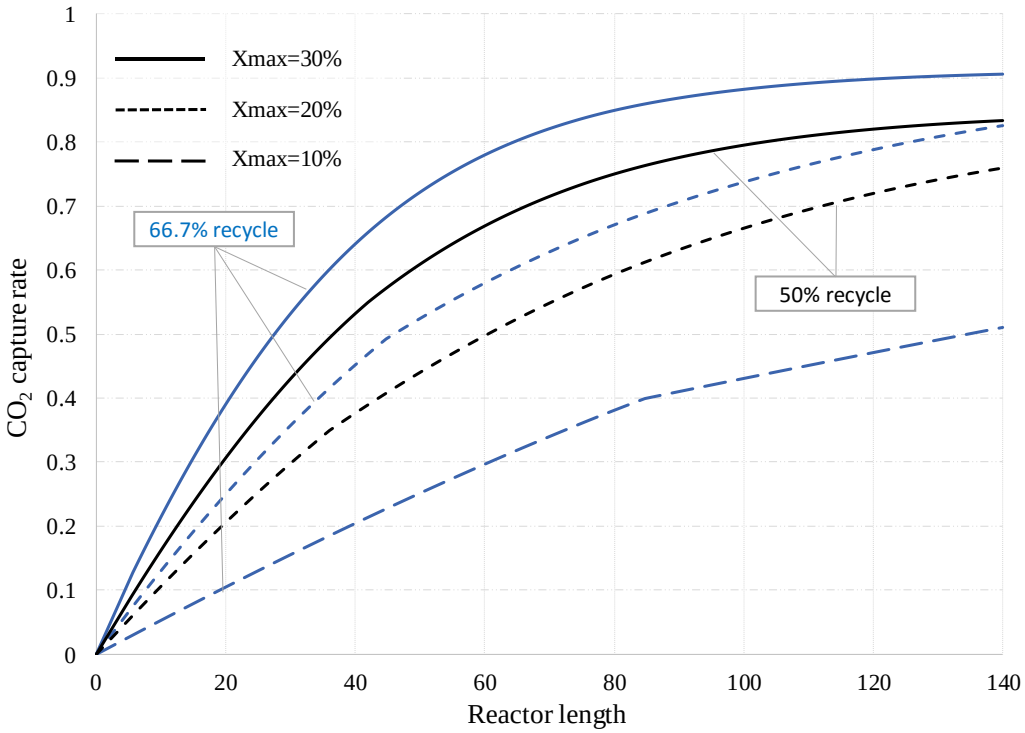

Figure 2.4: CO_2 capture efficiency vs. reactor length, for adiabatic reactor, solid feeding from the calciner of 5 kg/Nm^3 and different recycle ratios and X_{max}.

This project has received funding from the European Union's Horizon2020 Research and Innovation Programme under Grant Agreement No 641185

In Table 2.2, extended results of the CaL simulations are resumed. Cases 1-8 correspond to cases already discussed in the previous figures. In the last line the heat required in the calciner per kg of captured CO_2 for heating and calcination of the recarbonated raw meal is reported. As anticipated, high CO_2 capture efficiency and low calciner heat duty can be obtained by high solid loading in the carbonator and solids recycle. Sorbent capacity also influence the calcination heat duty significantly.

Case 9 is referred to a case where the carbonator inlet temperature is increased from 600 to 650°C. Compared to the corresponding case with same sorbent capacity and recycle rate and 600°C at carbonator inlet (i.e. case 5), CO_2 capture efficiency reduced by 5% points, indicating the importance of keeping a sufficiently low temperature at the carbonator inlet to enhance the reaction driving force for carbonation along the reactor.

Case 10 and 11 refer to the calculations of an adiabatic downflow reactor for X_{max} of 0.2 and 0.1, with a total length of 60 m and gas velocity of 4 m/s. Thanks to the increased residence times, CO_2 capture efficiency can be increased by 7 and 14% points compared to the corresponding gooseneck reactor cases 5 and 6.

Table 2.2: Results from the simulations of the entrained flow carbonator with different operating conditions, for a total reactor length of 140 m for the gooseneck reactor and 60 m for the downflow reactor.

Type of reactor	Adiabatic, gooseneck									Adiabatic, downflow	
Case #	1	2	3	4	5	6	7	8	9	10	11
Input variables:											
X_{max}	0.2	0.2	0.2	0.2	0.2	0.1	0.3	0.3	0.2	0.2	0.1
Inlet temperature, °C	600	600	600	600	600	600	600	600	650	600	600
Solids recycle, %	0	0	0	50	66.7	66.7	50	66.7	66.7	66.7	66.7
$m_{s,from\_calc}/V_g$, kg/Nm^3	5	10	15	5	5	5	5	5	5	5	5
$F_{Ca,from\_calc}/F_{CO2}$	6.6	13.2	19.8	6.6	6.6	6.6	6.6	6.6	6.6	6.6	6.6
Output variables:											
$m_{s,in\_react}/V_g$, kg/Nm^3	5	10	15	10.29	15.61	15.37	10.32	15.68	15.57	15.67	15.48
CO_2 capture eff., %	56.1	79.2	88.7	75.9	82.5	51.0	83.3	90.6	77.3	89.5	65.3
Outlet temperature, °C	723.8	649.9	678.3	692.1	668.9	643.7	713.7	675.1	713.7	679.8	659.9
G_s, kg/s m^2	24.2	47.7	71.1	49.0	73.8	72.1	49.3	74.2	69.5	19.8	19.4
$X_{out\ carb}$, %	8.6	6.1	4.6	11.6	12.6	7.9	12.7	13.8	11.8	13.7	10.0
Q_{calc}, kJ/kg$_{CO2,capt}$	8870	11871	15249	8234	8316	11541	7698	7845	7756	7813	9596

This project has received funding from the European Union's Horizon2020 Research and Innovation Programme under Grant Agreement No 641185

REFERENCES

[ABA, 2002] Abanades, J.C., 2002. The maximum capture efficiency of CO2 using a carbonation/calcination cycle of CaO/CaCO3. *Chem. Eng. J*, 90: 303-306.

[DEL, 2017] De Lena E., Spinelli M., Martínez I., Gatti M., Scaccabarozzi R., Cinti G., Romano M.C., 2017. Process integration study of tail-end Ca-Looping process for CO_2 capture in cement plants. *International Journal of Greenhouse Gas Control*, In press.

[GRA, 2006] Grasa, G.S., Abanades, J.C., 2006. CO2 Capture Capacity of CaO in Long Series of Carbonation/Calcination Cycles. *Ind Eng Chem Res*, 45: 8846-8851.

[GRA, 2008] Grasa, Abanades, Alonso, González, 2008. Reactivity of highly cycled particles of CaO in a carbonation/calcination loop. *Chem Eng J*, 137: 561-567

[GRA, 2009] G. Grasa, R. Murillo, M. Alonso, J.C. Abanades, Application of the random pore model to the carbonation cyclic reaction, AIChE J. 55 (2009) 1246–1255.

[GS, 2016] GS process simulation code. http://www.gecos.polimi.it/software/gs.php

[KUN, 1997] Kunii, D., Levenspiel, O., 1997. Circulating fluidized-bed reactors. *Chem Eng Sci*, 52: 2471-2482.

[MAR, 2013] Martínez, I., Grasa, G., Murillo, R., Arias, B., Abanades, J.C., 2013. Modelling the continuous calcination of $CaCO_3$ in a Ca-looping system. *Chemical Engineering Journal*, 215-216: 174-181.

[MAR, 2016] Martínez, I., Grasa, G., Parkkinen, J., Tynjälä, T., Hyppänen, T., Murillo, R., Romano, M.C., 2016. Review and research needs of Ca-Looping systems modelling for post-combustion CO2 capture applications. *International Journal of Greenhouse Gas Control*, 50: 271-304.

[PFE, 1966] R. Pfeffer, S. Rossetti, S. Lieblein, Analysis and correlation of heat-transfer coefficient and friction factor data for dilute gas-solid suspensions, NASA technical note, 1966.

[RAJ, 2006] K.S. Rajan, S.N. Srivastava, B. Pitchumani, B. Mohanty, Simulation of gas–solid heat transfer during pneumatic conveying: Use of multiple gas inlets along the duct, Int. Commun. Heat Mass Transf. 33 (2006) 1234–1242.

[RAJ, 2008] K.S. Rajan, K. Dhasandhan, S.N. Srivastava, B. Pitchumani, Studies on gas–solid heat transfer during pneumatic conveying, Int. J. Heat Mass Transf. 51 (2008) 2801–2813.

[ROM, 2012] Romano, 2012. Modeling the carbonator of a Ca-Looping process for CO_2 capture from power plant flue gas. *Chem Eng Sci*, 69: 257-269.

This project has received funding from the European Union's Horizon2020 Research and Innovation Programme under Grant Agreement No 641185